The Effects of Carbidopa on Uptake of 6-^{18}F-Fluoro-L-DOPA in PET of Pheochromocytoma and Extraadrenal Abdominal Paraganglioma

Henri J.L.M. Timmers[1,2], Mohiuddin Hadi[3], Jorge A. Carrasquillo[3], Clara C. Chen[3], Lucia Martiniova[1], Millie Whatley[3], Alexander Ling[4], Graeme Eisenhofer[5], Karen T. Adams[1], and Karel Pacak[1]

[1]Reproductive Biology and Medicine Branch, National Institute of Child Health and Human Development, National Institutes of Health, Bethesda, Maryland; [2]Department of Endocrinology, Radboud University Nijmegen Medical Centre, Nijmegen, The Netherlands; [3]Nuclear Medicine Department, Warren G. Magnuson Clinical Center, National Institutes of Health, Bethesda, Maryland; [4]Department of Diagnostic Radiology, Warren G. Magnuson Clinical Center, National Institutes of Health, Bethesda, Maryland; and [5]Clinical Neurocardiology Section, National Institute of Neurological Disorders and Stroke, National Institutes of Health, Bethesda, Maryland

6-^{18}F-fluoro-L-3,4-dihydroxyphenylalanine (^{18}F-DOPA) PET is a useful tool for the detection of certain neuroendocrine tumors, especially with the preadministration of carbidopa, an inhibitor of DOPA decarboxylase. Whether carbidopa also improves ^{18}F-DOPA PET of adrenal pheochromocytomas and extraadrenal paragangliomas is unknown. The aim of this study was to investigate the sensitivity of ^{18}F-DOPA PET in the detection of paraganglioma and its metastatic lesions and to evaluate whether tracer uptake by the tumors is enhanced by carbidopa. **Methods:** Two patients with nonmetastatic adrenal pheochromocytoma, and 9 patients with extraadrenal abdominal paraganglioma (1 nonmetastatic, 8 metastatic), underwent whole-body CT, MRI, baseline ^{18}F-DOPA PET, and ^{18}F-DOPA PET with oral preadministration of 200 mg of carbidopa. The dynamics of tracer uptake by these lesions and the physiologic distribution of ^{18}F-DOPA in normal tissues were recorded. **Results:** Seventy-eight lesions were detected by CT or MRI, 54 by baseline ^{18}F-DOPA PET ($P = 0.0022$ vs. CT/MRI), and 57 by ^{18}F-DOPA PET plus carbidopa ($P = 0.0075$ vs. CT/MRI, not statistically significant vs. baseline). In reference to findings on CT and MRI, the sensitivities of baseline ^{18}F-DOPA PET were 47.4% for lesions and 55.6% for positive body regions, versus 50.0% (lesions) and 66.7% (regions) for ^{18}F-DOPA PET plus carbidopa (neither is statistically significant vs. baseline). Compared with baseline, carbidopa detected additional lesions in 3 (27%) of 11 patients. Carbidopa increased the mean (±SD) peak standardized uptake value in index tumor lesions from 6.4 ± 3.9 to 9.1 ± 5.6 ($P = 0.037$). Pancreatic physiologic ^{18}F-DOPA uptake, which may mask adrenal pheochromocytoma, is blocked by carbidopa. **Conclusion:** Carbidopa enhances the sensitivity of ^{18}F-DOPA PET for adrenal pheochromocytomas and extraadrenal abdominal paragangliomas by increasing the tumor-to-background ratio of tracer uptake. The sensitivity of ^{18}F-DOPA PET for metastases of paraganglioma appears to be limited.

Received Apr. 12, 2007; revision accepted May 31, 2007.

For correspondence or reprints contact: Karel Pacak, MD, PhD, DSc, Reproductive Biology and Medicine Branch, National Institute of Child Health and Human Development, 10 Center Dr., Bldg. 10, CRC, RM 1-E 3140, MSC 1109, Bethesda, MD 20892-1109.

E-mail: karel@mail.nih.gov

Key Words: 6-fluoro-DOPA; 6-^{18}F-fluorodopamine; carbidopa; pheochromocytoma; paraganglioma; positron emission tomography; standardized uptake value; region of interest

J Nucl Med 2007; 48:1599–1606
DOI: 10.2967/jnumed.107.042721

Apart from its well-established role in the assessment of striatal dopaminergic function in Parkinson's disease (*1*), 6-^{18}F-fluoro-L-3,4-dihydroxyphenylalanine (^{18}F-DOPA) PET has emerged as a useful tool for the localization of gastrointestinal carcinoid tumors, a common form of neuroendocrine tumor (*2–5*). This examination is based on the capability of neuroendocrine tumors to take up, decarboxylate, and store amino acids, such as DOPA, and their biogenic amines (*6*). With respect to other neuroendocrine tumors, ^{18}F-DOPA PET studies have yielded promising results in the imaging of paraganglioma (*7–9*). Paragangliomas derive either from sympathetic tissue in adrenal and extraadrenal abdominal or thoracic locations or from parasympathetic tissue of the head and neck (*10*). A paraganglioma arising from the catecholamine-producing cells of the adrenal medulla is also commonly referred to as a pheochromocytoma (*11,12*).

^{18}F-DOPA PET of the brain is generally preceded by the oral administration of carbidopa, a peripheral aromatic amino acid decarboxylase inhibitor, which decreases the decarboxylation and subsequent renal clearance of ^{18}F-DOPA (*13*), thereby increasing tracer availability in the striatum (*14*). Carbidopa is also used to increase ^{18}F-DOPA uptake by tumor cells in the imaging of neuroendocrine tumors (*5,15*). Previous investigations of ^{18}F-DOPA PET in patients with paraganglioma did not include administration of carbidopa (*7,8*). As in functional imaging of other neuroendocrine tumors, carbidopa may largely improve the diagnostic performance of ^{18}F-DOPA PET in the localization of paraganglioma.

The aim of this study was to evaluate the usefulness of ^{18}F-DOPA PET in the localization of benign and malignant paraganglioma. Of primary interest was whether preadministration of carbidopa enhances the uptake of ^{18}F-DOPA by paraganglioma and improves diagnostic accuracy. In addition, the effects of carbidopa on the dynamics of tracer uptake by paraganglioma and the physiologic distribution of ^{18}F-DOPA in normal tissues were studied. Eleven patients with nonmetastatic (n = 3) or metastatic (n = 8) paraganglioma underwent ^{18}F-DOPA PET with and without preadministration of oral carbidopa.

MATERIALS AND METHODS

Patients

Between June and October 2006, 11 consecutive patients (6 men, 5 women) with a mean age (±SD) of 45.7 ± 7.6 y were evaluated 11.8 ± 8.1 y after a histologically confirmed diagnosis of adrenal pheochromocytoma or extraadrenal abdominal paraganglioma. Of these, 5 patients had an underlying mutation of the succinate dehydrogenase subunit B gene; 1 patient, of the succinate dehydrogenase subunit D gene; and 2 patients, of the "rearranged during transfection" oncogene. In 3 patients, the complete results of genetic testing are pending. Clinical details of individual patients are provided in Table 1. At the time of the PET studies, 3 patients had nonmetastatic paraganglioma: the first (patient 2) had an extraadrenal periaortic paraganglioma; the second (patient 5), a right adrenal pheochromocytoma; and the third (patient 9), a recurrent left adrenal pheochromocytoma. The remaining 8 patients had biochemical and radiologic evidence of metastatic extraadrenal abdominal paraganglioma, defined as the presence of metastatic lesions at sites where chromaffin tissue is normally absent (*16*). Systemic therapies, that is, either chemotherapy or ^{131}I-methyliodobenzylguanidine therapy (Table 1), if any, had been completed within a range of 11 mo to 9 y before the study.

The study protocol was approved by the Institutional Review Board of the National Institute of Child Health and Human Development at the National Institutes of Health. All patients provided written informed consent.

CT and MRI

CT of the neck, chest, abdomen, and pelvis was performed on all patients, using a LightSpeed Ultra (GE Healthcare), LightSpeed QX/i (GE Healthcare), or Mx8000 IDT (Philips) scanner. Section thickness was 2–2.5 mm in the neck and 5 mm through the chest, abdomen, and pelvis. Studies were performed with a rapid infusion of nonionic water-soluble contrast agent, as well as oral contrast material.

In 6 of 11 patients, MRI of the neck, chest, abdomen, or pelvis was performed, using a 1.5- or 3-T scanner (GE Healthcare and Philips). Phased-array coils were used for neck imaging, and either phased-array torso or quadrature body coils elsewhere. T1-weighted gradient-echo and short-τ inversion recovery or fat-suppressed fast spin-echo T2-weighted imaging parameters were adjusted so as to minimize examination time while achieving desired anatomic coverage. Image thickness was 5 mm for neck studies and 5–8 mm for other body regions. Preinjection images were obtained in the axial plane. Studies included injection of a gadolinium-diethylenetriaminepentaacetic acid contrast agent, using

TABLE 1
Patient Characteristics

Patient no.	Sex	Mutation	Age at diagnosis (y)	Location of primary tumor	Biochemical phenotype	Time to metastases* (y)	Locations of metastases	Previous treatment
1	M	SDHB	27	L extraadrenal abdominal	None	0	Abdominal LN, mediastinum, bone	Primary tumor resection; CVD
2	F	SDHB	51	R paraaortic abdominal	NE	—	—	MIBG
3	F	SDHB	23	Paraaortic abdominal	NE	0.3	Abdominal LN, bone	Primary tumor resection; CVD
4	M	SDHD	22	R adrenal	NE	10.3	Abdominal LN, liver, mediastinum, bone	Primary tumor resection; MIBG
5	F	Pending	53	R adrenal	NE	—	—	—
6	M	SDHB	10	R paraadrenal	NE + DA	8.4	Abdominal LN, lung, liver, bone, neck	MIBG
7	M	Pending	39	R adrenal	NE + DA	14.7	Abdominal LN, mediastinum, bone	Primary tumor resection
8	F	RET	33	R + L adrenal	NE + E	6.2	Abdominal LN, liver, bone	Primary tumor resection; MIBG
9	F	RET	33	R + L adrenal	E	—	—	Primary tumor resection
10	M	SDHB	40	L paraaortic	NE	3.9	Liver	Primary tumor resection
11	M	Pending	40	R adrenal	NE + DA	5.4	Lung, bone	Primary tumor resection; CVD; MIBG

*Time between diagnosis of primary tumor and metastatic disease.
SDHB/D = succinate dehydrogenase subunit B/D; LN = lymph nodes; CVD = cyclophosphamide/vincristine/dacarbazine; NE = norepinephrine; MIBG = ^{131}I-methyliodobenzylguanidine; DA = dopamine; RET = rearranged during transfection; E = epinephrine.

fat-suppressed T1-weighted gradient-echo imaging, generally in both axial and coronal planes.

^{18}F-DOPA PET

All patients underwent ^{18}F-DOPA PET. Before scanning, an index lesion was selected in each patient, based on previously performed CT or MRI. In cases of multiple metastases, the largest tumor was taken as the index (Table 2). Each patient underwent 2 ^{18}F-DOPA PET scans, 1–4 wk apart. The baseline scan was performed without carbidopa, and the second scan was preceded by oral administration of 200 mg of carbidopa, 1 h before tracer injection. The patients fasted for at least 4 h before the 1-min intravenous injection of 469 ± 12 MBq (12.67 ± 0.33 mCi) of ^{18}F-DOPA at baseline and 452 ± 22 MBq (12.20 ± 0.61 mCi, P = not statistically significant [NS] vs. baseline) after carbidopa. An Advance scanner (GE Healthcare) with a 15-cm axial field of view was used with a rod source attenuation correction. During the first 25 min after tracer injection, dynamic scanning at the level of the index lesion was performed by acquiring 12, 4, 4, and 7 frames of 5-, 15-, 30-, and 180-s durations, respectively. For subsequent whole-body scanning, 5-min emission images in the 2-dimensional mode from the top of the skull to the mid thigh were obtained, starting 30 min after tracer injection. After whole-body scanning, a delayed 5-min emission image was obtained at the level of the index tumor lesion, starting 105 min after tracer injection. PET images were reconstructed on a 256 × 256 matrix using an iterative algorithm provided by the manufacturer. Analysis was performed on attenuation-corrected images.

Analysis of Data

CT and MRI images were read by radiologists who were unaware of the results of ^{18}F-DOPA PET. Lesions detected by CT or MRI that were typical of or highly suggestive of paraganglioma were considered positive.

^{18}F-DOPA PET studies were each read independently, in a masked fashion, by 2 nuclear medicine physicians. Lesions were graded on a scale of 1–5 (1 = not paraganglioma, 2 = probably not paraganglioma, 3 = equivocal, 4 = probably paraganglioma, 5 = definitely paraganglioma). Lesions with scores of 4 and 5 were counted as positive findings. Discrepancies were resolved by consensus review.

Lesions on CT and MRI were counted in the following 3 separate body regions: neck, thorax, and abdomen/pelvis. The lesions that were counted included both soft-tissue and bone lesions. Coronally reprojected lesions on ^{18}F-DOPA PET using Medimage software were counted in the same regions and in an additional region, that is, the head. If the number of lesions in a region exceeded 10, the count was truncated at 10 to avoid bias toward that region. Total lesion counts per scan were calculated as the sum of separate region counts. Because the head was not scanned by CT and MRI, head lesions were excluded from the comparison of total lesion counts between CT or MRI and ^{18}F-DOPA PET. Apart from counting individual lesions, we compared the number of positive regions, that is, regions containing at least 1 lesion, between imaging modalities, again excluding the head region for comparison between CT or MRI and ^{18}F-DOPA PET. The sensitivity of ^{18}F-DOPA PET was calculated as the number of lesions and positive regions detected by ^{18}F-DOPA PET in reference to lesions and positive regions detected by CT or MRI as the gold standard.

Standardized uptake values (SUVs) corrected for the lean body mass were calculated (SUV = Bq/g per Bq injected × lean body mass). Regions of interest were manually drawn around the index tumor lesions and around the basal ganglia, lungs, myocardium, liver, kidneys, and—when visible—the pancreas. Throughout the article, SUV results refer to maximum SUV, unless stated otherwise. Time–activity curves of the index tumor lesions were constructed from appropriately thresholded regions of interest on early dynamic scanning and static images at the tumor level, using IDL software based on region-of-interest routines (ITT Visual Information Solutions). Peak SUVs and time to peak were obtained from interpolated curves using 4-point least-squares quadratic interpolation implemented in IDL.

TABLE 2
Tumor Detection

Parameter	CT or MRI	^{18}F-DOPA PET	
		Baseline	Carbidopa
Number of lesions			
Head	—	7	7
Neck	4	4	5
Chest	16	17	17
Abdomen/pelvis	58	33*	35*
Total, except head	78	54*	57*
Total, including head	—	61	64
Number of positive regions			
Head	—	4	4
Neck	3	2	2
Chest	5	4	4
Abdomen/pelvis	10	7	9
Total, except head	18	13	15
Total, including head	—	17	19

*$P < 0.01$ vs. CT or MRI.

Statistics

Results are given as mean ± SD unless stated otherwise. The McNemar test was used to compare the number of lesions and positive regions and sensitivities between different imaging modalities. SUVs, peak activities, and time intervals until peak activity were compared between ^{18}F-DOPA PET scans with and without carbidopa preadministration, using the paired Student t test. A 2-sided P value of less than 0.05 was considered significant. Statistical analysis was performed using Statistical Package for the Social Sciences (SPSS for Windows 12; SPSS Inc.).

RESULTS

Detection of Tumors

The interval between the baseline and carbidopa ^{18}F-DOPA PET scans was 1 wk in 9 patients, 2 wk in 1 patient (patient 6), and 4 wk in 1 patient (patient 1), depending on the availability of the PET scanner. One patient (patient 2), in whom the baseline ^{18}F-DOPA PET findings were negative, had inadvertently taken 40 mg instead of 200 mg of carbidopa before the second scan. This second scan was excluded from the analysis. Discrepant readings between the 2 nuclear physicians were solved by consensus for 4 lesions

on baseline ^{18}F-DOPA PET and 2 lesions on carbidopa ^{18}F-DOPA PET.

The locations of primary tumors and metastatic lesions detected by CT or MRI in individual patients are indicated in Table 1. In the 11 patients, 78 lesions in total were detected by CT or MRI, versus 54 lesions by baseline ^{18}F-DOPA PET ($P = 0.0022$ vs. CT/MRI) and 57 lesions by carbidopa ^{18}F-DOPA PET ($P = 0.0075$ vs. CT/MRI, NS vs. baseline ^{18}F-DOPA PET, Table 2). Carbidopa ^{18}F-FDOPA PET identified 1 neck lesion and 1 chest lesion that were missed by CT or MRI. The total numbers of positive body regions were 18 on CT or MRI, 13 on baseline ^{18}F-DOPA PET (P = NS vs. CT/MRI), and 15 on carbidopa ^{18}F-DOPA PET (P = NS vs. CT/MRI, P = NS vs. baseline ^{18}F-DOPA PET). These findings correspond to sensitivities of baseline ^{18}F-DOPA PET of 47.4% for individual lesions and 55.6% for positive regions. The sensitivities of carbidopa ^{18}F-DOPA PET were 50.0% for lesions and 66.7% for regions (both P = NS vs. baseline ^{18}F-DOPA PET).

Compared with baseline ^{18}F-DOPA PET, carbidopa pretreatment resulted in the detection of 3 additional lesions in 3 patients. In patient 1, in whom CT and MRI showed multiple metastases in the mediastinum and abdomen (lymph nodes and spine), baseline ^{18}F-DOPA PET did not show any abdominal lesions, whereas after carbidopa, the scan revealed pathologic activity in the lower abdomen. In patient 8, who had multiple metastatic lesions in the spine, liver, and abdominal lymph nodes, ^{18}F-DOPA PET showed 3 pathologic cervical spine foci at baseline, versus 4 after carbidopa pretreatment. In patient 9, a recurrent paraganglioma in the left adrenal bed was detected by CT, MRI, and ^{18}F-DOPA PET after carbidopa but not by baseline ^{18}F-DOPA PET. Baseline ^{18}F-DOPA PET was false-negative because the tumor was masked by physiologic uptake by the pancreas (Fig. 1). The diagnosis was later confirmed histologically.

Dynamic Studies of ^{18}F-DOPA Uptake by Index Tumor Lesions

All index tumor lesions were positive on ^{18}F-DOPA PET, except for the index liver lesion of patient 10. The time–activity curves of ^{18}F-DOPA uptake by the individual index tumor lesions at baseline, that is, without carbidopa, versus after carbidopa pretreatment are depicted in Figure 2. In 4 patients (patients 1, 4, 6, and 9), a brief peak in activity was observed within the first 2 min after tracer injection. These initial peaks were attributed to transient tracer flow in adjacent blood vessels or vascular tumor blush and were discarded from the analysis. In these 4 cases, the second, more persistent, peak was taken as the actual peak in tracer accumulation by tumor cells. Peak SUVs and time intervals until peak are indicated in Table 3. Mean peak activity ($\pm$SD) was higher after carbidopa (9.1 ± 5.6) than at baseline (6.4 ± 3.9, $P = 0.037$). Mean time interval ($\pm$SD) until peak was longer after carbidopa (85.2 ± 25.1 min) than at baseline (60.6 ± 34.7 min, $P = 0.010$).

Physiologic Uptake of ^{18}F-DOPA

Uptake of ^{18}F-DOPA by the basal ganglia, lungs, myocardium, and liver increased markedly after carbidopa administration, as indicated by significantly higher SUVs (Table 4). At baseline, the pancreas was clearly visible on ^{18}F-DOPA PET in all patients, whereas after carbidopa, the pancreas could not be discerned, except in 1 patient (patient 4). In this patient, maximum and mean pancreatic SUV decreased from 6.01 and 3.10 at baseline to 5.00 and 2.41 after carbidopa. Physiologic excretion into bile ducts, the gallbladder, and the urogenital system continued to be seen after carbidopa.

DISCUSSION

Compared with baseline ^{18}F-DOPA PET, oral preadministration of carbidopa resulted in the detection of additional lesions in 1 of 3 patients with nonmetastatic paraganglioma and in 2 of 8 patients with metastatic paraganglioma. Carbidopa enhanced the uptake of ^{18}F-DOPA by paraganglioma lesions and significantly blocked physiologic tracer uptake by the pancreas. Pancreatic uptake is a potential confounder in the detection of adrenal lesions. Despite carbidopa enhancement, however, only 50% of suspected tumor lesions detected by CT or MRI were positive on ^{18}F-DOPA PET.

^{18}F-DOPA PET of Paraganglioma

Paraganglioma can be localized using a very specific radiopharmaceutical such as ^{123}I-metaiodobenzylguanidine or ^{18}F-fluorodopamine, which are actively transported into neurosecretory granules of catecholamine-producing cells via the cell membrane norepinephrine transporter system (*17*). However, these highly specific tracers may yield false-negative results, especially in malignant paraganglioma (*18,19*). In the search for alternative imaging strategies for these tumors, we have found that ^{18}F-FDG PET is the preferred technique for localizing metastatic lesions of succinate dehydrogenase subunit B–related paraganglioma (*20*). In addition, others have shown that ^{18}F-DOPA PET provides an additional alternative for the functional imaging of sympathetic (*8*) and parasympathetic (*7*) paraganglioma. Like other neuroendocrine tumors, paraganglioma cells have the ability to take up, decarboxylate, and store amino acids and their biogenic amines (*6,17*). ^{18}F-labeled DOPA enters neuroendocrine tumor cells through the membranous amino acid transporter. Hyperproduction of catecholamines in paraganglioma cells occurs via decarboxylation of DOPA into dopamine and subsequent conversion into norepinephrine and epinephrine (*21*). Therefore, compared with noncatecholamine-secreting neuroendocrine tumors, paraganglioma is theoretically expected to be particularly well targeted by ^{18}F-DOPA–based imaging.

In a previous study of 17 patients with nonmetastatic adrenal and extraadrenal sympathetic paraganglioma, ^{18}F-DOPA PET detected tumors with a strikingly high sensitivity and specificity of 100% for both (*8*). Our study of

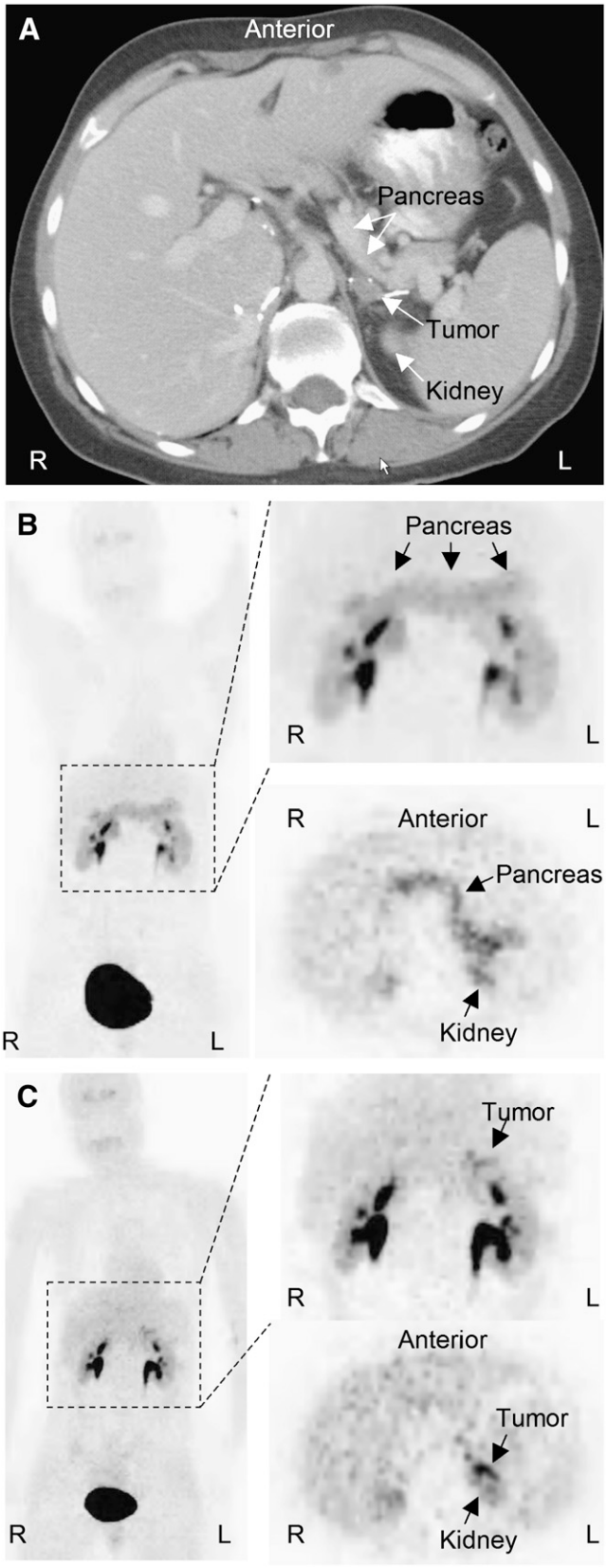

FIGURE 1. CT scan (A) and ^{18}F-DOPA PET scans without carbidopa (B) and after carbidopa (C) in patient 9. In PET scans, anterior reprojected images are at left, details of anterior reprojected images are at top right, and transverse sections at tumor level are at bottom right. CT scan shows (recurrent) tumor in left adrenal bed, near tail of pancreas, consistent with abnormal left adrenal focus on ^{18}F-DOPA PET after carbidopa. On baseline ^{18}F-DOPA PET, left adrenal bed is masked by physiologic uptake by pancreas.

patients with predominantly metastatic paraganglioma suggests a lesion-based sensitivity for ^{18}F-DOPA PET of only 50%. A possible explanation for this discrepancy is that ^{18}F-DOPA uptake is higher in primary nonmetastatic tumors than in metastatic lesions. Theoretically, results may also have been influenced by a relative overrepresentation in our group of patients with paraganglioma due to an underlying gene mutation, that is, mainly of succinate dehydrogenase subunit B. In addition, we used lesions detected by CT and MRI as our gold standard for sensitivity calculations of ^{18}F-DOPA PET. CT and MRI have been shown to have an excellent sensitivity (>90%) for paraganglioma but to lack specificity (*22*). Therefore, false-positive lesions on anatomic imaging may have unfairly lowered our estimates of ^{18}F-DOPA PET sensitivity. Histologic confirmation of disease would be the ideal standard of reference, but for obvious reasons, surgery or biopsy of all lesions on CT and MRI is not feasible. Furthermore, lesion counts may be discrepant when multiple adjacent lesions on CT or MRI are counted as individual lesions but are not discriminated as separate lesions by ^{18}F-DOPA PET because of limitations in resolution.

The performance of ^{18}F-DOPA PET in the localization of paraganglioma has not been systematically compared with that of other functional imaging modalities. In the previously mentioned study by Hoegerle et al. (*8*), a subset of the patients also underwent ^{123}I-metaiodobenzylguanidine scanning, which yielded a sensitivity of 71%. We are currently conducting a large study for head-to-head comparison of ^{18}F-DOPA PET, ^{123}I-metaiodobenzylguanidine scintigraphy, ^{18}F-fluorodopamine PET, and ^{18}F-FDG PET in patients with paraganglioma.

Effects of Carbidopa on ^{18}F-DOPA PET of Paraganglioma

^{18}F-DOPA PET protocols for the evaluation of the central dopaminergic system and carcinoid tumors often include oral preadministration of 100–250 mg of carbidopa. This agent decreases peripheral ^{18}F-DOPA decarboxylation and subsequent renal clearance of ^{18}F-DOPA metabolites (*13*), thereby increasing tracer availability and uptake by target tissues, such as the basal ganglia (*14*) and carcinoid tumors (*5,15*), thus improving the quality of imaging. The present findings clearly indicate that carbidopa also enhances the uptake of ^{18}F-DOPA by paraganglioma. Dynamic curves of ^{18}F-DOPA uptake by index tumor lesions show a considerable increase in peak activity. Moreover, carbidopa-enhanced scanning revealed additional paraganglioma lesions in one third of patients, compared with baseline ^{18}F-DOPA PET.

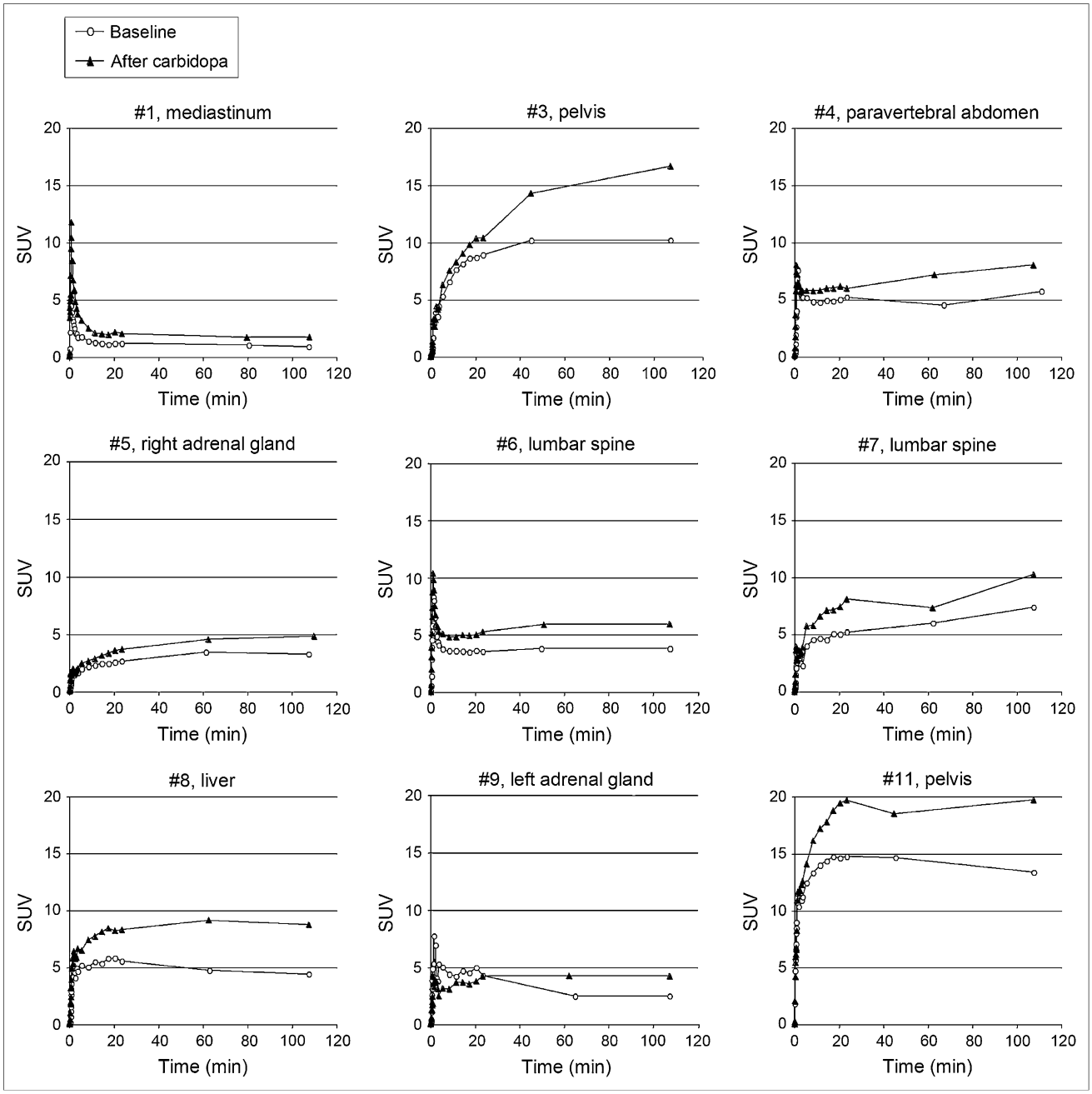

FIGURE 2. Dynamics of ^{18}F-DOPA tumor uptake. Time–activity curves of ^{18}F-DOPA uptake by index lesions at baseline (no carbidopa) vs. after carbidopa. Patient numbers and locations of index lesions are indicated in graph titles.

A potential limitation of ^{18}F-DOPA PET in the detection of adrenal paraganglioma is the substantial physiologic uptake in the pancreas. Other pitfalls of ^{18}F-DOPA PET of paraganglioma include tracer accumulation in the gallbladder and renal collecting system, mimicking an extraadrenal tumor (*23*). In the present study, we showed that masking of a pheochromocytoma could be prevented by blockade of pancreatic uptake by carbidopa. A decrease in the pancreatic uptake of the tracers ^{18}F-DOPA and ^{11}C-5-hydroxytryptophan by carbidopa has been previously reported (*15,24*). The mechanism by which carbidopa blocks tracer accumulation in the pancreas is unknown. De Lonlay et al. have speculated that pancreatic visualization is due to intracellular decarboxylation of ^{18}F-DOPA into ^{18}F-dopamine and subsequent intracellular "trapping" of ^{18}F-dopamine, and that inhibition of DOPA decarboxylase by carbidopa in the pancreas may result in diffusion of ^{18}F-DOPA back from the cell into the extracellular space and prevention of intracellular accumulation of ^{18}F-dopamine (*24*). In their immunohistochemical studies, low DOPA decarboxylase levels were found (*24*). We postulate that in paraganglioma cells, both the decarboxylase enzyme and transmembrane amino acid transporters are upregulated as part of overactive secretory pathways, similar to observations in other

TABLE 3
Dynamics of ^{18}F-DOPA Tumor Uptake

Patient no.	Location of index lesion	Time to peak (min)		Peak SUV	
		Baseline	Carbidopa	Baseline	Carbidopa
1	Mediastinum	24	24	1.2	2.1
3	Pelvis	77	90	10.8	17.2
4	Paravertebral abdomen	107*	107*	5.5	8.0
5	R adrenal gland	79	101	3.5	4.8
6	Lumbar spine	80	81	3.9	6.2
7	Lumbar spine	107*	107*	7.3	10.2
8	Liver	20	74	5.9	9.2
9	L adrenal gland	19	76	4.7	4.3
11	Pelvis	32	107*	14.7	19.7
Mean ± SD		60.6 ± 34.7	85.2 ± 25.1†	6.4 ± 3.9	9.1 ± 5.6†

*Uptake curve was still rising at last imaging time point.
†$P < 0.05$ vs. baseline.

neuroendocrine tumors (*25,26*). In paraganglioma, the competitive inhibition by carbidopa of intrinsically upregulated decarboxylase may therefore be only partial and may be outweighed by larger tracer availability and uptake, resulting in a net increase in tracer accumulation. Similarly, variability in intrinsic DOPA decarboxylase activity among tumors may explain why some paragangliomas are detected by ^{18}F-DOPA PET and others are not.

Administration of carbidopa and ^{18}F-DOPA, which in this setting represents off-label use, was well tolerated by the patients. Koopmans et al. have reported a patient with metastatic carcinoid in whom a carcinoid crisis was triggered by rapid injection of ^{18}F-DOPA after oral administration of carbidopa (*27*). We did not observe any signs or symptoms relating to a surge in catecholamine release by the tumors, such as palpitations, sweating, or headache. With respect to acquisition parameters for carbidopa-enhanced ^{18}F-DOPA PET of paraganglioma, the time–activity curves suggest that most patients reach 85% of the maximal tumor uptake within 30 min and thus imaging could commence at 30 min after injection. However, imaging at later times is also possible since there is very little release of the tracer from tumor over the 105 min of imaging. Our results are in line with a previous report on ^{18}F-DOPA PET in neuroendocrine tumors indicating no advantage of a 90-min scan over a 30-min scan with respect to either visual interpretation or lesion SUVs (*2*).

CONCLUSION

The sensitivity of ^{18}F-DOPA PET for the localization of paraganglioma is improved by preadministration of carbidopa, which enhances the uptake of ^{18}F-DOPA by paraganglioma lesions and allows better discrimination between paraganglioma and physiologic tracer uptake by normal surrounding tissues. However, this initial study in malignant paraganglioma also suggests that the sensitivity of ^{18}F-DOPA PET for detecting metastatic lesions is limited.

ACKNOWLEDGMENTS

This research was supported by the Intramural Research Program of the NICHD/NIH. We thank Jacques Lenders of the Department of General Internal Medicine, Radboud University Nijmegen Medical Center, Nijmegen, the

TABLE 4
Physiologic Distribution of ^{18}F-DOPA

Location	Maximum SUV		Mean SUV	
	Baseline	Carbidopa	Baseline	Carbidopa
Basal ganglia	2.43 ± 0.55	3.73* ± 0.81	1.28 ± 0.31	2.04* ± 0.43
Myocardium	2.53 ± 0.57	3.18* ± 0.64	0.75 ± 0.16	1.04* ± 0.22
Lungs	0.69 ± 0.24	0.88* ± 0.24	0.22 ± 0.08	0.29* ± 0.07
Liver	3.13 ± 0.75	3.42 ± 0.64	1.3 ± 0.34	1.48* ± 0.28
Kidneys	5.33 ± 1.51	5.32 ± 1.47	2.51 ± 0.66	2.43 ± 0.71
Pancreas	6.21 ± 1.79	—	3.03 ± 1.04	—

*$P < 0.01$ vs. baseline.

Netherlands, for helpful discussions and feedback on the manuscript.

REFERENCES

1. Snow BJ, Tooyama I, McGeer EG, et al. Human positron emission tomographic [^{18}F]fluorodopa studies correlate with dopamine cell counts and levels. *Ann Neurol.* 1993;34:324–330.
2. Becherer A, Szabo M, Karanikas G, et al. Imaging of advanced neuroendocrine tumors with ^{18}F-FDOPA PET. *J Nucl Med.* 2004;45:1161–1167.
3. Hoegerle S, Altehoefer C, Ghanem N, et al. Whole-body ^{18}F dopa PET for detection of gastrointestinal carcinoid tumors. *Radiology.* 2001;220:373–380.
4. Nanni C, Rubello D, Fanti S. ^{18}F-DOPA PET/CT and neuroendocrine tumours. *Eur J Nucl Med Mol Imaging.* 2006;33:509–513.
5. Koopmans KP, de Vries EG, Kema IP, et al. Staging of carcinoid tumours with ^{18}F-DOPA PET: a prospective, diagnostic accuracy study. *Lancet Oncol.* 2006;7: 728–734.
6. Pearse AG. The cytochemistry and ultrastructure of polypeptide hormone-producing cells of the APUD series and the embryologic, physiologic and pathologic implications of the concept. *J Histochem Cytochem.* 1969;17:303–313.
7. Hoegerle S, Ghanem N, Altehoefer C, et al. ^{18}F-DOPA positron emission tomography for the detection of glomus tumours. *Eur J Nucl Med Mol Imaging.* 2003;30:689–694.
8. Hoegerle S, Nitzsche E, Altehoefer C, et al. Pheochromocytomas: detection with ^{18}F DOPA whole body PET—initial results. *Radiology.* 2002;222:507–512.
9. Brink I, Schaefer O, Walz M, Neumann HP. Fluorine-18 DOPA PET imaging of paraganglioma syndrome. *Clin Nucl Med.* 2006;31:39–41.
10. DeLellis RA, Lloyd RV, Heitz PU, Eng C. *Pathology and Genetics: World Health Organization Classification of Tumours of Endocrine Organs.* Oxford, U.K.: Oxford University Press; 2004.
11. Pacak K, Keiser H, Eisenhofer G. Pheochromocytoma. In: DeGroot LS, Jameson JL, eds. *Textbook of Endocrinology.* 5th ed. Philadelphia, PA: Elsevier, Inc.; 2005:2501–2534.
12. Lenders JW, Eisenhofer G, Mannelli M, Pacak K. Phaeochromocytoma. *Lancet.* 2005;366:665–675.
13. Brown WD, Oakes TR, DeJesus OT, et al. Fluorine-18-fluoro-L-DOPA dosimetry with carbidopa pretreatment. *J Nucl Med.* 1998;39:1884–1891.
14. Hoffman JM, Melega WP, Hawk TC, et al. The effects of carbidopa administration on 6-[^{18}F]fluoro-L-dopa kinetics in positron emission tomography. *J Nucl Med.* 1992;33:1472–1477.
15. Orlefors H, Sundin A, Lu L, et al. Carbidopa pretreatment improves image interpretation and visualisation of carcinoid tumours with ^{11}C-5-hydroxytryptophan positron emission tomography. *Eur J Nucl Med Mol Imaging.* 2006;33: 60–65.
16. Linnoila RI, Keiser HR, Steinberg SM, Lack EE. Histopathology of benign versus malignant sympathoadrenal paragangliomas: clinicopathologic study of 120 cases including unusual histologic features. *Hum Pathol.* 1990;21:1168–1180.
17. Eisenhofer G. The role of neuronal and extraneuronal plasma membrane transporters in the inactivation of peripheral catecholamines. *Pharmacol Ther.* 2001;91:35–62.
18. van der Harst E, de Herder WW, Bruining HA, et al. [^{123}I]Metaiodobenzylguanidine and [^{111}In]octreotide uptake in benign and malignant pheochromocytomas. *J Clin Endocrinol Metab.* 2001;86:685–693.
19. Mamede M, Carrasquillo JA, Chen CC, et al. Discordant localization of 2-[^{18}F]-fluoro-2-deoxy-D-glucose in 6-[^{18}F]-fluorodopamine- and [^{123}I]-metaiodobenzylguanidine-negative metastatic pheochromocytoma sites. *Nucl Med Commun.* 2006;27:31–36.
20. Timmers HJ, Kozupa K, Chen CC, et al. Superiority of fluorodeoxyglucose positron emission tomography to other functional imaging techniques in the evaluation of metastatic SDHB-associated pheochromocytoma and paraganglioma. *J Clin Orthod.* 2007. In press.
21. Eisenhofer G, Huynh TT, Hiroi M, Pacak K. Understanding catecholamine metabolism as a guide to the biochemical diagnosis of pheochromocytoma. *Rev Endocr Metab Disord.* 2001;2:297–311.
22. Maurea S, Cuocolo A, Reynolds JC, Neumann RD, Salvatore M. Diagnostic imaging in patients with paragangliomas: computed tomography, magnetic resonance and MIBG scintigraphy comparison. *Q J Nucl Med.* 1996;40:365–371.
23. Balan KK. Visualization of the gall bladder on F-18 FDOPA PET imaging: a potential pitfall. *Clin Nucl Med.* 2005;30:23–24.
24. de Lonlay P, Simon-Carre A, Ribeiro MJ, et al. Congenital hyperinsulinism: pancreatic [^{18}F]fluoro-L-dihydroxyphenylalanine (DOPA) positron emission tomography and immunohistochemistry study of DOPA decarboxylase and insulin secretion. *J Clin Endocrinol Metab.* 2006;91:933–940.
25. Gilbert JA, Bates LA, Ames MM. Elevated aromatic-L-amino acid decarboxylase in human carcinoid tumors. *Biochem Pharmacol.* 1995;50:845–850.
26. Meijer WG, Copray SC, Hollema H, et al. Catecholamine-synthesizing enzymes in carcinoid tumors and pheochromocytomas. *Clin Chem.* 2003;49:586–593.
27. Koopmans KP, Brouwers AH, De Hooge MN, et al. Carcinoid crisis after injection of 6-^{18}F-fluorodihydroxyphenylalanine in a patient with metastatic carcinoid. *J Nucl Med.* 2005;46:1240–1243.